



Antimony Complexes for Electrocatalysis: Activity of a Main-Group Element in Proton Reduction

Jianbing Jiang[†], Kelly L. Materna[†], Svante Hedström[†], Ke R. Yang, Robert H. Crabtree,*
Victor S. Batista,* and Gary W. Brudvig*

Abstract: Main-group complexes are shown to be viable electrocatalysts for the H₂-evolution reaction (HER) from acid. A series of antimony porphyrins with varying axial ligands were synthesized for electrocatalysis applications. The proton-reduction catalytic properties of TPSb(OH)₂ (TP = 5, 10, 15, 20-tetra(*p*-tolyl)porphyrin) with two axial hydroxy ligands were studied in detail, demonstrating catalytic H₂ production. Experiments, in conjunction with quantum chemistry calculations, show that the catalytic cycle is driven via the redox activity of both the porphyrin ligand and the Sb center. This study brings insight into main group catalysis and the role of redox-active ligands during catalysis.

Environmental concerns and fossil fuel depletion have prompted a search for sustainable energy sources. H₂ is a viable energy carrier since it has a high energy density (142 MJ kg⁻¹),^[1] forms only water upon combustion, and is carbon-neutral.^[1] Platinum is a very efficient catalyst for the H₂-evolution reaction (HER);^[2] however, replacement with cheaper alternatives is desirable. Molecular HER catalysts are advantageous because their properties are readily tuned by structural modifications, and mechanistic studies are easier to perform under homogenous catalytic conditions.^[3] Though great progress has been made in the area, improving the catalytic efficiency, acid stability, and electrocatalytic overpotentials^[3] may require a broader exploration of catalyst structures.

Compared to transition-metal catalysts, main-group elements have not been extensively explored; although the reported studies have revealed benefits, there are still rather few catalytic applications.^[4] An innovation that may help is the use of redox-active ligands.^[5] In this case, the ligand becomes redox-active, and the main-group element, which could be redox-active or not, acts as the substrate-binding site. This contrasts with transition-metal catalysis, where the metal

has both functions. Redox-active ligands can have a role in multi-electron reactions by facilitating electron transfer to or from the catalyst, thus playing an important role in the overall catalytic mechanism.^[5] Here, we report porphyrin complexes of antimony as HER catalysts. Sb complexes are known to perform photocatalytic oxidations.^[6,7] However, to the best of our knowledge, this is the first time that molecular Sb complexes have been used for catalytic reduction. In this work, we demonstrate that Sb-porphyrin complexes function as electrocatalysts for efficient proton reduction. Furthermore, a combination of experiments and quantum chemical calculations show that both the porphyrin ligand and the Sb center are redox-active during electrocatalysis,^[8] which has not been observed in previously reported antimony catalytic systems.

The synthesis, purification, and characterization of three Sb^V-porphyrin complexes (Figure 1) are described in the Supporting Information (Scheme S1). The photophysical properties of these Sb-porphyrin complexes, studied by absorption spectroscopy, were dependent on the ligand set (Supporting Information, Table S1 and Figure S1).

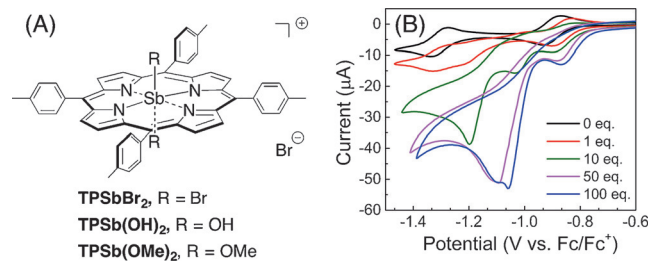


Figure 1. A) Structures of the Sb-porphyrin complexes. B) TFA-dependent CV of 0.5 mM TPSb(OH)₂ in 0.1 M TBAPF₆ in acetonitrile; glassy carbon working electrode; 50 mVs⁻¹ scan rate.

The electrochemical properties of TPSb(OH)₂ were explored using cyclic voltammetry (CV). CV measurements were performed in acetonitrile using a 0.1M tetrabutylammonium hexafluorophosphate (TBAPF₆) electrolyte and a 0.5 mM porphyrin electrocatalyst. Under reducing conditions, TPSb(OH)₂ (Supporting Information, Figure S2A) has two reversible reduction waves at -0.89 V and -1.30 V vs. Fc/Fc⁺ indicative of reductions of the porphyrin ligand; the first reduction forms the porphyrin radical anion and the second forms the porphyrin dianion.^[9,10] This is corroborated by density functional theory (DFT) calculations, which show that the first two reduction events sequentially reduce the porphyrin ring twice, with calculated potentials of -0.86 V

[*] Dr. J. Jiang,^[†] K. L. Materna,^[†] Dr. S. Hedström,^[†] Dr. K. R. Yang, Prof. R. H. Crabtree, Prof. V. S. Batista, Prof. G. W. Brudvig
Department of Chemistry, Yale University
New Haven, CT 06520 (USA)

and
Energy Sciences Institute, Yale University
West Haven, CT 06516 (USA)
E-mail: robert.crabtree@yale.edu
victor.batista@yale.edu
gary.brudvig@yale.edu

[†] These authors contributed equally to this work.

Supporting information and the ORCID identification number(s) for the author(s) of this article can be found under:
<https://doi.org/10.1002/anie.201704700>.

and -1.31 V vs. Fc/Fc^+ , using the free-base TP as an internal reference. The frontier orbitals and spin density of $\text{TPSb}(\text{OH})_2$ in its various oxidation states are shown in the Supporting Information, Figure S3. Experimental plots of peak current versus square root of the scan rate are linear, indicative of diffusional processes (Supporting Information, Figure S2). A summary of experimental and calculated electrochemical properties of the porphyrins can be found in the Supporting Information, Table S1.

To screen the catalytic capability of the Sb porphyrins for proton-reduction catalysis, CV measurements were performed using 0.5 mM $\text{TPSb}(\text{OH})_2$ with increasing concentrations of trifluoroacetic acid (TFA) ($0, 1, 10, 50$, and 100 equiv) as the proton source (Figure 1B). An additional irreversible peak appears upon addition of TFA that increases as the acid concentration increases, which we attribute to proton-reduction catalysis.^[11–13]

To better understand the catalytic system, several control experiments were conducted, including measurements on blank electrolyte solutions (with TFA) and the free-base porphyrin TP in the presence of TFA. These control experiments explicitly demonstrate the involvement of the Sb center in the catalysis (Supporting Information, Figure S4A,B). Additionally, several voltammetric control experiments were performed to further verify the occurrence of proton reduction, and exclude reduction of the $-\text{CF}_3$ or $-\text{CO}_2^-$ moieties of TFA (Supporting Information, Figure S4C). Lastly, to demonstrate that the increase in current was not due to an Sb salt produced by demetalation of the porphyrin, CVs of 0.5 mM $\text{Sb}(\text{OAc})_3$ were collected with 100 equiv of TFA. The CVs did not show an increase in current, but in fact a decrease in current, demonstrating that the Sb salt was not able to act as a proton-reduction catalyst and that demetalation was not responsible for activity (Supporting Information, Figure S4D). Sb salts also have low solubility in acetonitrile and we did not observe any precipitation during catalysis. Taken together, the control experiments strongly suggest that the observed catalytic activity is from the Sb-porphyrin species.

To confirm and quantify the formation of H_2 , GC was employed. An electrochemical cell containing a high-surface-area carbon paper working electrode, an Ag/AgCl pseudoreference electrode, and a Pt wire auxiliary electrode (separated from the working compartment by a frit) were used during electrolysis of 0.5 mM $\text{TPSb}(\text{OH})_2$ with 200 equiv of TFA. CVs were collected prior to electrolysis, showing the catalytic peak upon addition of acid (Supporting Information, Figure S6A). Electrolysis was performed by holding the potential at the catalytic peak voltage for 2 h. The chronoamperogram during the electrolysis shows a steady current at about -2 mA (Supporting Information, Figure S6B) with a slow rise in reductive current after 90 min. During the electrolysis, the headspace of the electrochemical cell was sampled by injecting 200 μL into the GC at $36, 91$, and 120 min. The formation of H_2 was confirmed and compared to a pure H_2 injection (Supporting Information, Figures S5, S8). A Faradaic efficiency of 62% was found by comparing the H_2 gas production (43.3 μmol) during 2 h vs. the theoretical value, calculated from the charge passed. During 2 h of

electrolysis, $\text{TPSb}(\text{OH})_2$ performed 9 catalytic turnovers with a turnover frequency of 4.3 h^{-1} . To produce further evidence that $\text{TPSb}(\text{OH})_2$ was forming H_2 , an electrolysis of a control sample with a bare electrode under the same conditions was also performed. The chronoamperogram shows a significantly lower current (ca. -50 μA) and less H_2 (6.7 μmol) production than with $\text{TPSb}(\text{OH})_2$ (Supporting Information, Figures S6C, S7B).

The observed increase in reductive current after 90 min of electrolysis of $\text{TPSb}(\text{OH})_2$ indicated that another species may be forming, which could account for the relatively low Faradaic yield. To probe this, UV/Vis spectroscopy was used to monitor any changes in $\text{TPSb}(\text{OH})_2$ during electrolysis. No changes in the UV/Vis spectrum were observed upon the addition of 200 equiv of TFA to 0.5 mM $\text{TPSb}(\text{OH})_2$ prior to electrolysis (Supporting Information, Figures S10). During electrolysis, three new peaks at $440, 503$, and 667 nm appear in the UV/Vis spectrum (Figure 2), which suggests reduction of the porphyrin ring.^[14] Based on these results, we propose that the reductive current that is not involved in H_2 formation instead drives the formation of the reduced porphyrin species.^[15–18]

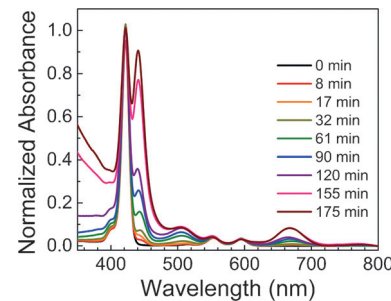


Figure 2. UV/Vis spectra of a solution of $\text{TPSb}(\text{OH})_2$ with 200 equiv of TFA after electrolysis for 0 – 175 min.

Because molecular electrocatalysts can be prone to decomposition and binding to electrodes, X-ray photoelectron spectroscopy (XPS) was performed on a rinsed carbon paper electrode post electrolysis of $\text{TPSb}(\text{OH})_2$.^[19] Sb was detected on the carbon paper electrode, and the XPS spectra were compared to that of $\text{TPSb}(\text{OH})_2$ deposited on carbon paper by the drop-cast method. The $\text{TPSb}(\text{OH})_2$ peaks are at a higher binding energy than the post-electrolysis Sb features, suggesting that the electrodeposited species is a mixture of two reduced Sb tetrapyrrole species; the N 1s XPS spectra, representing the state of the porphyrin ligand, also show a broadened N peak compared to the drop-cast $\text{TPSb}(\text{OH})_2$, suggesting that more than one species is present on the electrode (Supporting Information, Figure S9b).^[20–22] To gain further insight into the nature of the species deposited on the electrode surface, a carbon paper electrode was soaked for 2 h in a solution of $\text{TPSb}(\text{OH})_2$ in acetonitrile, mimicking the solvent environment during catalysis. No Sb was detected by XPS under these conditions, suggesting that $\text{TPSb}(\text{OH})_2$ does not bind to the electrode (Supporting Information, Figure S9A), but rather only the reduced porphyrin species deposits. Additionally, drop-cast $\text{TPSb}(\text{OH})_2$ readily desorbs

from the C paper when soaked in methanol (Supporting Information, Figure S9A), retaining the same UV/Vis spectrum. Lastly, the presence of Sb^0 at 528.0 eV was not observed in the post-electrolysis sample (Figure 3), precluding the possibility of porphyrin demetalation during electrolysis.^[23]

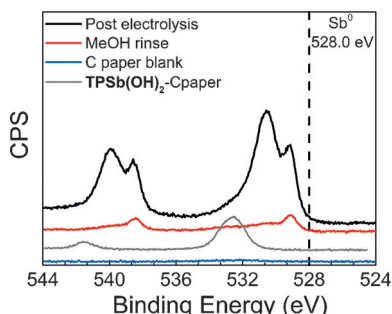


Figure 3. XPS spectra of the carbon paper after electrolysis (black), after rinsing the post-electrolysis carbon paper with MeOH for 22 h (red), blank carbon paper (blue), and drop-cast TPSb(OH)₂ on carbon paper (gray). The left peaks are from Sb 3d_{3/2} and the right peaks are from Sb 3d_{5/2}. The O 1s peak overlaps the right peak.

To further characterize the nature of the Sb on the surface, the post-electrolysis carbon paper was soaked in methanol for 22 h to desorb the species on the surface, and a UV/Vis spectrum was collected, which showed Soret and Q-bands that differ from TPSb(OH)₂ (Supporting Information, Figure S11). XPS spectra of the carbon paper post methanol rinsing also showed a decrease in surface-bound Sb (Figure 3). Taken together, the UV/Vis desorption spectrum and the XPS results provide strong evidence that the compound on the surface is a reduced Sb-tetrapyrrole species. The surface-adsorbed species and its possible catalytic activity were further characterized by CVs and chronoamperograms (Supporting Information, Figure S12). The lower current suggests that the reduced species on the electrode surface is less active than TPSb(OH)₂ during catalysis. Regardless, it is clear that Sb-tetrapyrrole compounds are capable of performing proton-reduction catalysis.

The experimental results support the DFT catalytic cycle described in Figure 4 A (see the Supporting Information for computational details). First, a one-electron reduction occurs to activate the pre-catalyst, forming the Sb^V-porphyrin-radical anion species **I2** consistent with the first reversible peak in the CV with TFA (Figure 1B). Because the UV/Vis and ¹H NMR spectra of TPSb(OH)₂ are not affected by the presence of TFA (Supporting Information, Figures S10 and S13), initial ligand protonation is ruled out before species **I1** is reduced (Figure 4A). The free energy change of protonating **I2** by TFA is +9.7 kcal mol⁻¹, suggesting that the singly reduced species **I2** is not basic enough to efficiently advance the catalysis. Further reduction of **I2** with a second electron yields **I3**, and the protonation of **I3** with TFA has an associated free energy change of only +1.7 kcal mol⁻¹, which is small enough to move forward with sufficient TFA concentration. The protonated species **I4** loses an axial water ligand to form intermediate **I5** in a strongly exergonic step. **I5** is the active catalyst that enters the catalytic cycle (Figure 4). The

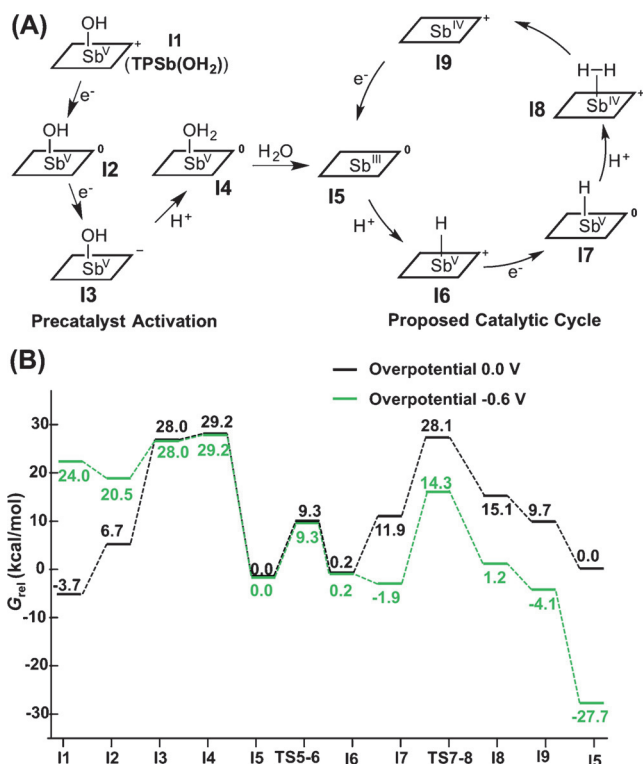


Figure 4. A) Proposed catalytic cycle. The charge near each porphyrin ring is the total charge of the species. B) DFT free energies of intermediates **I1**-**I9** in the cycle, and activation free energies of the two protonation steps. The potential of the incoming electrons is referenced relative to the reaction $\text{CF}_3\text{COOH} + \text{e}^- \rightarrow \text{CF}_3\text{COO}^- + \frac{1}{2}\text{H}_2$ for the 0.0 V overpotential case (black). For the -0.6 V overpotential case, 600 meV is subtracted from the free energy changes of the steps involving electrochemical reduction (green).

oxidation state Sb^{III} of **I5** is supported by the presence of a doubly occupied MO (HOMO-2 in the Supporting Information, Figures S14-S20) corresponding to an Sb 5s lone pair, residing opposite the remaining OH axial ligand. The increase of Sb-N bond lengths from **I4** to **I5** is consistent with the experimental ionic radius increase from Sb^V (0.74 Å) to Sb^{III} (0.90 Å).^[24]

The active catalyst **I5** begins the catalytic cycle by accepting a proton with its 5s lone pair, forming the Sb^V-H hydride intermediate **I6**. The formation of **I6** is practically isoergic (+0.2 kcal mol⁻¹), with an activation free energy of 9.3 kcal mol⁻¹. This intermediate finds many analogues in various metal hydride species, occurring as intermediates in proton reduction catalysis.^[11-13] The calculated Sb-H bond length in **I6** is 1.70 Å, and the calculated charge of the H is -0.24 e, based on an atomic polar tensor charge analysis. The reduction of **I6** requires 11.7 kcal mol⁻¹. Like **I2**, the incoming electron populates the porphyrin ring rather than the metal center, because the two axial ligands obstruct the formation of an Sb lone pair. Protonation of the reduced hydride **I7**^[25] forms the H₂-bound complex **I8** with a free energy change of +3.2 kcal mol⁻¹ and an activation free energy of 16.2 kcal mol⁻¹. The H-H bond length in **I8** is 0.76 Å, which is very similar to an isolated H₂ molecule. On the other hand, the distance between Sb and H₂ is about 3.3 Å, indicating a very

weak interaction compared to transition-metal–dihydrogen complexes.^[26] The oxidation state of Sb in **I8** is best described as Sb^{IV}, as indicated by the Sb–N bond lengths as well as a singly occupied 5s orbital (Supporting Information, Figures S14–S21). The release of H₂ from **I8** is thermodynamically favored by 5.4 kcal mol⁻¹, yielding the intermediate **I9** that can be easily reduced to regenerate **I5**, completing the catalytic cycle. It is worth noting the important role of the axial ligands: with two axial ligands present, the porphyrin ring bears the reducing charge (in **I2**, **I3**, **I4**, and **I7**), whereas with a single axial ligand, the Sb can support a lone pair and be reduced to Sb^{IV} and Sb^{III} (**I5**, **I8**, and **I9**).

Because axial ligand substitutions are key steps in the proposed catalytic cycle (Figure 4), Sb-porphyrin complexes with different axial ligands (TPSb(OMe)₂ and TPSbBr₂; Figure 1A) were prepared and studied to probe how the ligands affect the electrochemical and catalytic efficiencies. By variation of the axial ligands, the electrochemical properties of TPSb(OMe)₂ and TPSbBr₂ (Supporting Information, Figure S22) showed significant tunability of the electronic properties (up to ca. 210 mV for the first reduction peak, and ca. 90 mV for the second one), compared to those of the benchmark molecule TPSb(OH)₂. This is of particular interest because these axial ligands are not directly bound to the porphyrin ring, which as described earlier bears the charge from a majority of the reduction steps. Nonetheless, our results clearly show that the Sb atom, along with acting as the catalytic center, is crucially responsible for mediating the interactions between the redox-active porphyrin ligand and the electronically non-innocent axial ligands, one of which is the hydride intermediate in the catalytic cycle.

To investigate the capabilities of TPSb(OMe)₂ and TPSbBr₂ for proton-reduction catalysis, CVs were collected under the same conditions as for TPSb(OH)₂ (Supporting Information, Figure S22). Both of these Sb complexes showed an irreversible peak upon addition of TFA, similar to that observed for TPSb(OH)₂, indicating that catalysis is occurring.^[11–13] The increase in magnitude of the current at the catalytic peak is similar among all three porphyrins, suggesting that their capacities for proton-reduction catalysis are comparable.

We predict that the redox potential of the ligand can be tuned by variation of the polypyrrole type and substitution pattern, changes that are not expected to significantly affect the substrate-binding site. This advantage is not shared by classical HER catalysts in which the redox-active and substrate-binding sites are one and the same.

In conclusion, we have prepared a series of Sb-porphyrin complexes, and demonstrated their capability for proton-reduction catalysis. Our proposed catalytic mechanism is supported by both experiments and DFT free-energy and transition-state calculations. The catalytic activity of one molecule, (TPSb(OH)₂), is studied in particular detail. The effects of different axial ligands on the electrochemical properties and catalytic efficiencies are also studied, resulting in highly promising tunability of properties by facile structural modifications. To our knowledge, this is the first study using molecular complexes with Sb as the catalytic center for proton reduction. In a wider perspective, this work demon-

strates the viability of employing main-group elements for catalytic processes relevant for sustainable energy production, as well as the important role of redox-active ligands. This opens up new avenues for the application of compounds from cheaper elements beyond the transition-metal series.

Experimental Section

Details on instruments, experimental, control experiments, additional electrochemical and spectroscopic data, GC chromatograms, complexes with different axial ligands, DFT calculations, the two considered catalytic cycles, calculated frontier orbitals and spin densities, optimized xyz coordinates, and sample Gaussian input file can be found in the Supporting Information.

Acknowledgements

This work was supported by the U.S. Department of Energy, Chemical Sciences, Geosciences, and Biosciences Division, Office of Basic Energy Sciences, Office of Science (DE-FG02-07ER15909). Additional support was provided by a generous gift from the TomKat Foundation. We thank the Yale West Campus Analytical Core for help with NMR and MALDI-MS measurements. Computational resources were provided by the Yale Center for Research Computing.

Conflict of interest

The authors declare no conflict of interest.

Keywords: antimony · electrocatalysis · main-group elements · porphyrins · proton reduction

How to cite: *Angew. Chem. Int. Ed.* **2017**, *56*, 9111–9115
Angew. Chem. **2017**, *129*, 9239–9243

- [1] L. Schlapbach, A. Zettler, *Nature* **2001**, *414*, 353.
- [2] T. Abe, K. Hirano, Y. Shiraiishi, N. Toshima, M. Kaneko, *Eur. Polym. J.* **2001**, *37*, 753.
- [3] T. Stoll, C. E. Castillo, M. Kayanuma, M. Sandroni, C. Daniel, F. Odobel, J. Fortage, M.-N. Collomb, *Coord. Chem. Rev.* **2015**, *304*–305, 20.
- [4] P. P. Power, *Nature* **2010**, *463*, 171.
- [5] O. R. Luca, R. H. Crabtree, *Chem. Soc. Rev.* **2013**, *42*, 1440.
- [6] M. Ertl, E. Wöb, G. Knör, *Photochem. Photobiol. Sci.* **2015**, *14*, 1826.
- [7] T. Shiragami, J. Matsumoto, H. Inoue, M. Yasuda, *J. Photochem. Photobiol. C* **2005**, *6*, 227.
- [8] J. S. Jones, F. P. Gabbaï, *Acc. Chem. Res.* **2016**, *49*, 857.
- [9] H. Isago, Y. Kagaya, *Bull. Chem. Soc. Jpn.* **1996**, *69*, 1281.
- [10] Y. H. Liu, M. F. Benassy, S. Chojnacki, F. D’Souza, T. Barbour, W. J. Belcher, P. J. Brothers, K. M. Kadish, *Inorg. Chem.* **1994**, *33*, 4480.
- [11] D. K. Bediako, B. H. Solis, D. K. Dogutan, M. M. Roubelakis, A. G. Maher, C. H. Lee, M. B. Chambers, S. Hammes-Schiffer, D. G. Nocera, *Proc. Natl. Acad. Sci. USA* **2014**, *111*, 15001.
- [12] Y. Han, H. Fang, H. Jing, H. Sun, H. Lei, W. Lai, R. Cao, *Angew. Chem. Int. Ed.* **2016**, *55*, 5457; *Angew. Chem.* **2016**, *128*, 5547.
- [13] H. Lei, H. Fang, Y. Han, W. Lai, X. Fu, R. Cao, *ACS Catal.* **2015**, *5*, 5145.
- [14] M. Taniguchi, J. S. Lindsey, *Chem. Rev.* **2016**, *115*, 6534.

- [15] B. H. Solis, A. G. Maher, D. K. Dogutan, D. G. Nocera, S. Hammes-Schiffer, *Proc. Natl. Acad. Sci. USA* **2016**, *113*, 485.
- [16] A. M. Manke, K. Geisel, A. Fetzer, P. Kurz, *Phys. Chem. Chem. Phys.* **2014**, *16*, 12029.
- [17] M. Liu, C. Y. Chen, A. K. Mandal, V. Chandrashaker, R. B. Evans-Storms, J. B. Pitner, D. F. Bocian, D. Holten, J. S. Lindsey, *New J. Chem.* **2016**, *40*, 7721.
- [18] A. K. Mandal, T. Sahin, M. Liu, J. S. Lindsey, D. F. Bocian, D. Holten, *New J. Chem.* **2016**, *40*, 9648.
- [19] B. D. McCarthy, C. L. Donley, J. L. Dempsey, *Chem. Sci.* **2015**, *6*, 2827.
- [20] W. E. Morgan, W. J. Stec, J. R. Van Wazer, *Inorg. Chem.* **1973**, *12*, 953.
- [21] T. Birchall, J. A. Connor, L. H. Hillier, *J. Chem. Soc. Dalton Trans.* **1975**, 2003.
- [22] C. D. Wagner, *Faraday Discuss. Chem. Soc.* **1975**, *60*, 291.
- [23] R. I. Hegde, S. R. Sainkar, S. Badrinarayanan, A. P. B. Sinha, *J. Electron Spectrosc. Relat. Phenom.* **1981**, *24*, 19.
- [24] R. D. Shannon, *Acta Crystallogr. Sect. A* **1976**, *32*, 751.
- [25] Via DFT calculation, thermodynamic hydricity (hydride donor ability) values of **I6** and **I7** in CH₃CN are 66 and 46 kcal mol⁻¹, respectively. Owing to an increased negative charge on the porphyrin, the calculated thermodynamic hydricity value of **I7** is smaller than that of **I6**. The thermodynamic hydricity value of **I7** is comparable to that of HCO₃⁻ (44 kcal mol⁻¹; see Table 5 in Wiedner et al., *Chem. Rev.* **2016**, *116*, 8655), suggesting that this Sb-hydride system might be able to catalyze CO₂ reduction to give formate.
- [26] R. H. Crabtree, *Chem. Rev.* **2016**, *116*, 8750.

Manuscript received: May 7, 2017

Accepted manuscript online: June 19, 2017

Version of record online: July 4, 2017